Methods for Determining Stability in Continuum Elastic Rod Models of DNA

By Kathleen A. Hoffman

Department of Mathematics & Statistics,
University of Maryland, Baltimore County, USA

Elastic rod models of DNA have offered an alternative method for studying the macroscopic properties of the molecule. An essential component of the modelling effort is to identify the biologically accessible, or stable, solutions. The underlying variational structure of the elastic rod model can be exploited to derive methods that identify stable equilibrium configurations. We present two methods for determining the stability of the equilibria of elastic rod models: the conjugate point method and the distinguished diagram method. Additionally, we apply these methods to two intrinsically curved DNA molecules: a DNA filament with an A-tract bend and a DNA minicircle with a CAP binding site. The stable solutions of these models provide visual insight into the three-dimensional structure of the DNA molecules.

Keywords: Stability, Elastic Rod Model, Conjugate Points, Distinguished Bifurcation Diagrams

1. Introduction

Since the discovery of the double helical structure of DNA's two sugar-phosphate chains (Watson & Crick 1953), the molecule has been the focus of study by numerous scientists. Mechanical models of DNA have offered a new perspective for studying the macroscopic properties of the molecule. In particular, elastic rod models have been widely used as an approximation to DNA (Olson 1996; Schlick 1995, and references therein) and have led to new experiments. The elastic rod model consists of a framed curve where the curve, or centerline of the rod, runs through the middle of the double helix and one of the normal components of the frame points to one of the sugar-phosphate chains of the DNA molecule.

One important aspect of modelling is to determine which equilibria of the elastic rod model correspond to biologically realistic solutions and which ones do not, that is, which equilibrium points are actually minima of the energy functional. Critical points, the set of all possible minima, are solutions to the Euler-Lagrange equations. In order to identify which critical points are actually minima, we define an index corresponding to the number of linearly independent directions in which the functional decreases at the critical point. Thus, minima correspond to critical points with index zero. Determining the index, or stability of equilibria, is a central element of the classic theory of calculus of variations. However, for inextensible-unshearable elastic rods, the model has integral (isoperimetric) constraints and the classic theory cannot be applied directly. We discuss two particular methods for

determining the indices of these constrained critical points: the conjugate point method and the distinguished diagram method. The distinguished diagram method relies on the shape of the curve of solutions in a particular projection of the bifurcation diagram to track changes in the index. The conjugate point method for constrained calculus of variations problems is an extension of the ideas pioneered by Jacobi for unconstrained calculus of variations problems. While the conjugate point method focuses on determining the index of a particular solution, the distinguished diagram method tracks changes in the index of families of solutions.

There are, of course, many other techniques for determining stability of elastic rods and choosing the appropriate technique depends on the particular properties of the model. Some models describe the dynamic stability of the molecule over time (see, for example, Goriely & Tabor 1997*a*, *b*, *c*), while others focus on static equilibrium of the energy. This paper focuses on stability results available for static equilibria of inextensible, unshearable elastic rod models of DNA. Classical methods, such as perturbation theory, have been used to determine the onset of instability of the planar, isotropic, uniform elastic loop with straight unstressed state as imposed twist is increased. The circular solution is stable for imposed twist less than $2\pi\sqrt{3}/\gamma$, where γ represents the ratio of twisting stiffness to bending stiffness (see for example, Benham 1989; Guitter and Leibler 1992; Le Bret 1979; Mitchell 1889; Zajac 1962). Le Bret (1984) proposed a more general necessary condition $d(Lk)/d(Wr) \geq 0$, where Lk and Wr are two independent quantities connected via the formula $Lk = Tw + Wr$, and Tw is the twist. Tobias et al. (2000) extended Le Bret's result to include impenetrable elastic rods (Coleman *et al.* 2000; Jülicher 1994; LeBret 1984; Tobias *et al.* 2000; van der Heijden *et al.* 2003), as well as proposed several other necessary conditions, which in combination comprise a sufficient condition for stability. The condition $d(Lk)/d(Wr) \geq 0$ can be obtained using similar techniques to those used to derive the distinguished diagram method with the additional assumption that the elastic rod is naturally straight with uniform twist. In van der Heijden *et al.* (2003), stability is determined from load-deflection diagrams for clamped rods both with and without self-contact effects and Neukirch *et al.* (2002) uses the same diagrams to study an instability jump for infinite to finite length rods. These diagrams are equivalent to the distinguished diagrams presented here. The conjugate point method has been applied to anisotropic elastic rods with inherent curvature, as demonstrated in Manning & Hoffman (2001), where the stability of an elastic loop was determined as a function of increasing curvature. Examples of a DNA filament and a DNA minicircle modelled as an isotropic uniform elastic rod with inherent curvature and twist will be presented in §5 to illustrate the distinguished diagram method and the conjugate point method.

2. Variational Formulation of the Elastic Rod Model

(*a*) *The Energy Functional*

In this section, we develop a variational formulation of the elastic rod model of DNA, that is, we derive an elastic energy functional, whose minima we define to be stable configurations of the model. Specifically, we adopt the special Cosserat theory of elastic rods (Antman 1995). The configuration of an elastic rod is described by a centerline $\mathbf{r}(s)$ (written as a function of arclength $s \in [0,1]$) and directors

$\{\mathbf{d}_1(s), \mathbf{d}_2(s), \mathbf{d}_3(s)\}$ that form an orthonormal frame describing the orientation of the cross-section of the rod. Although this formulation assumes an elastic rod of unit length, this assumption in no way restricts the length of the DNA molecule represented by this model since the formulation and results remain valid (with proper rescaling) for an elastic rod with arbitrary length. Figures $1c, d$ and $2b, c$ display two configurations of twisted elastic rods. The centerline of the rod $\mathbf{r}$ is illustrated as a curve and the path of one of the directors $\mathbf{d}_1$ is shown using the ribbon along the curve. This is sufficient to determine the entire frame of directors since we restrict our attention to the particular case of inextensible and unshearable rods, for which $\mathbf{d}_3(s)$, the director perpendicular to the cross-section, coincides with the tangent vector to the centerline:

$$\mathbf{r}'(s) \equiv \frac{\mathrm{d}\mathbf{r}(s)}{\mathrm{d}s} = \mathbf{d}_3(s). \tag{2.1}$$

Elastic rod models with this assumption have been shown to be a good approximation for DNA where the forces are below a certain threshold for significant DNA extension (Smith et al. 1996). Although the unshearability-inextensibility assumption would seem to simplify the problem by restricting the class of elastic rods that we consider, it introduces integral constraints. These constraints are derived by integrating the inextensibility-unshearability condition (2.1) to get

$$\int_0^1 \mathbf{d}_3 \, \mathrm{d}s = \mathbf{r}(1) - \mathbf{r}(0). \tag{2.2}$$

The stresses acting across a cross-section of the rod can be averaged to yield a net force $\mathbf{n}(s)$ and moment $\mathbf{m}(s)$ of the material in $s+$ acting on the material in $s-$. The components

$$m_i(s) \equiv \mathbf{m}(s) \cdot \mathbf{d}_i(s), \quad i = 1, 2, 3,$$

of the moment $\mathbf{m}$ in the director frame play a role in the distinguished diagram method for rods described in §4; m_1 and m_2 are bending moments, and m_3 is the twisting moment.

Orthonormality of the directors $\{\mathbf{d}_i(s)\}$ implies the existence of a (Darboux) vector $\mathbf{u}(s)$ defined by the kinematic relations

$$\mathbf{d}_i'(s) = \mathbf{u}(s) \times \mathbf{d}_i(s), \qquad i = 1, 2, 3.$$

We denote the components of $\mathbf{u}$ in the rod frame by $u_i(s) \equiv \mathbf{u}(s) \cdot \mathbf{d}_i(s)$. The u_i are the *strains* in the model and determine the shape of the elastic rod up to translations and rotations of the configurations. Analogous functions $\hat{u}_1(s)$, $\hat{u}_2(s)$, and $\hat{u}_3(s)$ can be used to describe inherent bending and twisting of the rod that may be present even without external loading, as is the case with many DNA models. For instance, it is well-known that the double-helical structure of B-form DNA experiences a full twist approximately every 10.5 base-pairs and elastic rod models of DNA reflect this through the function $\hat{u}_3$. Similarly, the natural curvature of a DNA molecule would be represented in the elastic rod model through the functions $\hat{u}_1$ and $\hat{u}_2$.

The local energy cost in deforming from the unstressed shape is given by a strain energy density function W, whose integral over the length of the rod gives the total

strain energy:

$$E \equiv \int_0^1 W(u_j - \hat{u}_j, s)\, \mathrm{d}s. \tag{2.3}$$

One could assume a quite general dependence of W on the strains, but we have chosen to specialise to a quadratic energy, $W(u_j - \hat{u}_j, s) \equiv \left\{ \sum_{j=1}^{3} \frac{1}{2} K_j(s)[u_j - \hat{u}_j(s)]^2 \right\}$, which has proven accurate for many DNA configurations. The stability methods discussed in §3 and §4 are valid for more general forms of the elastic energy, however, for certain specific examples, the calculation of the index may simplify for quadratic energy.

The positive *stiffness* functions $K_j(s)$ and the unstressed strains $\hat{u}_j(s)$ are required input parameters to the model. One of the challenges of modelling DNA is to extract values for these parameters from experimental DNA data. For this information, we summarize results from Manning *et al.* (1996). According to the best available measurements, the stiffnesses are independent of s, that is, $K_i(s) = K_i$. The examples presented in §5 assume an isotropic rod, that is, equal bending stiffnesses: $K_1 = K_2$. This assumption seemingly contradicts the commonly held intuition of a prefered local bending direction of DNA. However, it has been shown that an anisotropic rod ($K_1 \neq K_2$) with a rapid twist averages to yield an effective isotropic ($K_1 = K_2$) rod on sufficiently large length scales (Kehrbaum & Maddocks 2000; Rey & Maddocks 2000). The appropriate value of $K_1 = K_2$ can be estimated based on sedimentation, light scattering, and cyclisation experiments (Hagerman 1988). The value of K_3 is more difficult to pinpoint and a range of values for the ratio $\gamma \equiv K_3/K_1$ appears in the literature (typically $0.5 \leq \gamma \leq 2.4$) (Schlick 1995; Moroz & Nelson 1998; Bouchiat & Mezard 2000). It is interesting to note that the stability of the elastic rod equilibria depend on the value of γ.

It is well known that, depending on the base-pair sequencing, certain molecules have significantly curved unstressed shapes. The unstressed strains $\hat{u}_i(s)$ can be determined from DNA sequencing information by appropriate filtering and smoothing techniques (Manning *et al.* 1996). In §5, two DNA molecules with inherent bends are constructed using sequencing information for A-tracts and CAP binding sites. This technique of filtering and smoothing is used to arrive at a continuum elastic rod model of those particular molecules.

Thus far, the variational formulation has been presented in a coordinate-free formulation, but in order to specify the boundary conditions on the rod, and calculate the first and second derivatives of the functional, the coordinate system of the moving frame of directors must be related to the fixed frame in space using a rotation matrix. In many problems in mechanics, this rotation matrix is parametrized by Euler angles. This is impractical for certain models of DNA involving nonplanar configurations because Euler angles necessarily have a singular direction. Instead, we parametrize the rotation matrix by four Euler parameters, that do not have a singular direction. The penalty for avoiding this singular direction is enforcing the unit length requirement on the Euler parameters. This restriction will manifest itself in the second variation of the functional in that it must be projected to allow only those variations that respect this constraint. We note that the strains u_i and the directors $\mathbf{d}_i$ can be represented as polynomial functions of the Euler parameters (see Dichmann 1994, for these explicit representations). Thus, in terms of the Euler parameters, the general variational problem that describes the twisted elastic rod

model of DNA is

$$E = \int_0^1 \frac{1}{2} \left\{ \sum_{i=1}^{3} K_i(s) \Big[u_i(\mathbf{q}, \mathbf{q}') - \hat{u}_i(s) \Big]^2 \right\} \, \mathrm{d}s,$$
$$\text{subject to} \quad \int_0^1 \mathbf{g}(\mathbf{q}) \, \mathrm{d}s = \mathbf{0}, \tag{2.4}$$
$$\mathbf{q}(0) = \langle 0, 0, 0, 1 \rangle, \quad \mathbf{q}(1) = \langle 0, 0, \sin(\alpha/2), \cos(\alpha/2) \rangle \equiv \mathbf{f}(\alpha),$$

where α is the imposed twist, and $\mathbf{g}(\mathbf{q}) \in \mathbb{R}^n$ depends on the specific DNA configuration.

For example, twisted elastic loops represent cyclized DNA. Cyclisation of DNA occurs when both the centerline and directors close: $\mathbf{r}(0) = \mathbf{r}(1), \quad \mathbf{d}_i(0) = \mathbf{d}_i(1)$, however, we have found it more convenient to compute a family of configurations using numerical continuation (Dichmann *et al.* 1996). Using this method, we consider the more general problem in which the centerline $\mathbf{r}$ and tangent director $\mathbf{d}_3$ close, but the normal directors are twisted by an angle α relative to their position at $s = 0$. Because of the closure of the centerline, the isoperimetric (integral) constraint is: $\int_0^1 \mathbf{d}_3(\mathbf{q}) \, \mathrm{d}s = \mathbf{r}(1) - \mathbf{r}(0) = \mathbf{0}$. Thus, in terms of Euler parameters, the specific variational problem that models twisted DNA minicircles is of the form (2.4) with $\mathbf{g}(\mathbf{q}) = \mathbf{d}_3(\mathbf{q})$. The boundary conditions on $\mathbf{q}$ at $s = 0$ orient the frame of directors $\mathbf{d}_1, \mathbf{d}_2, \mathbf{d}_3$ along the standard axes. At $s = 1$, the frame is rotated about $\mathbf{d}_3(0)$ by an angle α.

Another example is the elastic rod model of twisted DNA filaments, that are described by (2.4) with

$$\mathbf{g}(\mathbf{q}) = (\mathbf{d}_3(\mathbf{q}) \cdot \mathbf{e}_1, \mathbf{d}_3(\mathbf{q}) \cdot \mathbf{e}_2)^T,$$

where $\mathbf{e}_i$ represents the standard unit vectors. This model describes an elastic rod with the $s = 0$ end fixed at the origin, tangent to the z-axis. The $s = 1$ end of the rod lies on and tangent to the z-axis and twisted by an angle α with respect to the $s = 0$ end.

(*b*) *The Second Variation*

According to the standard multiplier rule for constrained variational problems, an associated functional

$$J[\mathbf{q}] = \int_0^1 \left(\left\{ \sum_{j=1}^{3} \frac{1}{2} K_j(s) [u_j(\mathbf{q}, \mathbf{q}') - \hat{u}_j(s)]^2 \right\} + \mathbf{g}^T \boldsymbol{\lambda} \right) \, \mathrm{d}s \equiv \int_0^1 L(\mathbf{q}, \mathbf{q}', s) \, \mathrm{d}s$$

is constructed. Constrained critical points are solutions of the standard Euler-Lagrange equations associated with the functional J

$$-\frac{\mathrm{d}}{\mathrm{d}s} L_{\mathbf{q}'} + L_{\mathbf{q}} = \mathbf{0}, \tag{2.5}$$

with the multiplier $\boldsymbol{\lambda}_0$ determined by solving (2.5) along with the constraints equations. There is an extensive literature on obtaining solutions to these equations for

the elastic rod model of DNA (see, for example, Dichmann et al. 1996, Manning *et al.* 1998, Hoffman *et al.* 2002) which we do not attempt to review. Instead, for the purposes of demonstrating methods that determine the stability of these equilibria, we assume that a family of solutions has already been computed.

Classification of these critical points involves an analysis of the second variation of J, namely

$$\delta^2 J[\delta\mathbf{q}] = \frac{1}{2}\int_0^1 \left[(\delta\mathbf{q}')^T\hat{\mathbf{P}}\delta\mathbf{q}' + (\delta\mathbf{q}')^T\hat{\mathbf{C}}^T\delta\mathbf{q} + \delta\mathbf{q}^T\hat{\mathbf{C}}\delta\mathbf{q}' + \delta\mathbf{q}^T\hat{\mathbf{Q}}\delta\mathbf{q}\right]\,\mathrm{d}s, \quad (2.6)$$

where $\hat{\mathbf{P}} = W_{\mathbf{q}'\mathbf{q}'}$, $\hat{\mathbf{C}} = W_{\mathbf{q}\mathbf{q}'}$, and $\hat{\mathbf{Q}} = \mathbf{g}^T_{\mathbf{q}\mathbf{q}}\boldsymbol{\lambda}_0 + W_{\mathbf{q}\mathbf{q}}$ are all s-dependent 4×4 matrices evaluated at $\mathbf{q}_0(s)$, a solution of the Euler-Lagrange equations (2.5). Here, we note that the second variation $\delta^2 J$ identically vanishes for variations of the form $\delta\mathbf{q} = c\mathbf{q}_0(s)$, for some $c\in\mathbb{R}$. These flat directions are artefacts of the parametrization of the rotation matrices using Euler parameters and are of no interest in determining stability of extremals. Therefore, we project the four-dimensional variations $\delta\mathbf{q}$ onto a space of three-dimensional variations $\boldsymbol{\zeta} = \boldsymbol{\Pi}(\delta\mathbf{q})$, that are pointwise orthogonal to $\mathbf{q}_0(s)$ (see Manning *et al.* 1998 for more details), and satisfy the linearized boundary conditions

$$\boldsymbol{\zeta}(0) = \mathbf{0} = \boldsymbol{\zeta}(1). \quad (2.7)$$

The second variation takes the same form:

$$\delta^2 J[\boldsymbol{\zeta}] = \frac{1}{2}\int_0^1 \left[(\boldsymbol{\zeta}')^T\mathbf{P}\boldsymbol{\zeta}' + \boldsymbol{\zeta}^T\mathbf{C}\boldsymbol{\zeta}' + (\boldsymbol{\zeta}')^T\mathbf{C}^T\boldsymbol{\zeta} + \boldsymbol{\zeta}^T\mathbf{Q}\boldsymbol{\zeta}\right]\mathrm{d}s, \quad (2.8)$$

but with

$$\begin{aligned}\mathbf{P} &= \boldsymbol{\Pi}W_{\mathbf{q}'\mathbf{q}'}\boldsymbol{\Pi}^T,\\ \mathbf{Q} &= \boldsymbol{\Pi}'W_{\mathbf{q}'\mathbf{q}'}(\boldsymbol{\Pi}')^T + \boldsymbol{\Pi}W_{\mathbf{q}\mathbf{q}}\boldsymbol{\Pi}^T + \boldsymbol{\Pi}\left(\mathbf{g}^T_{\mathbf{q}\mathbf{q}}\boldsymbol{\lambda}_0\right)\boldsymbol{\Pi}^T + 2\boldsymbol{\Pi}W_{\mathbf{q}\mathbf{q}'}(\boldsymbol{\Pi}')^T,\\ \mathbf{C} &= \boldsymbol{\Pi}'W_{\mathbf{q}'\mathbf{q}'}\boldsymbol{\Pi}^T + \boldsymbol{\Pi}W_{\mathbf{q}\mathbf{q}'}\boldsymbol{\Pi}^T.\end{aligned} \quad (2.9)$$

We also remark that Legendre's strengthened condition holds, that is, the matrix $\mathbf{P}$ is positive definite.

With the boundary conditions on $\boldsymbol{\zeta}$, an alternate form of the second variation is achieved after an integration by parts:

$$\delta^2 J[\boldsymbol{\zeta}] \;=\; \frac{1}{2}\int_0^1 \boldsymbol{\zeta}^T\mathcal{S}\boldsymbol{\zeta}\,\mathrm{d}s,$$

where $\mathcal{S}$ is the self-adjoint, second-order differential operator:

$$\mathcal{S}\boldsymbol{\zeta} \equiv -\frac{\mathrm{d}}{\mathrm{d}s}\left[\mathbf{P}\boldsymbol{\zeta}' + \mathbf{C}^T\boldsymbol{\zeta}\right] + \mathbf{C}\boldsymbol{\zeta}' + \mathbf{Q}\boldsymbol{\zeta}. \quad (2.10)$$

Admissible variations $\boldsymbol{\zeta}$ must also satisfy the linearized constraints

$$\int_0^1 \boldsymbol{\zeta}^T\mathbf{T}_i\,\mathrm{d}s = 0,\;\; i = 1,\ldots,n, \quad \text{where} \quad \mathbf{T}_i \equiv \boldsymbol{\Pi}\frac{\partial g_i}{\partial\mathbf{q}}(\mathbf{q}_0). \quad (2.11)$$

We assume that the $\mathbf{T}_i(s)$ are linearly independent (as functions of s) on every interval $(0, \sigma)$ for $0 < \sigma < 1$, as is the case for both examples of elastic rod models of DNA minicircles and DNA filaments.

A necessary condition for $\mathbf{q}_0$ to realise a constrained local minimum is (cf. Hestenes 1966)

$$\delta^2 J[\boldsymbol{\zeta}] \geq 0, \tag{2.12}$$

for all variations that satisfy the boundary conditions (2.7) and the linearized constraints (2.11). Two practical methods for determining if this necessary condition holds for isoperimetrically constrained problems, such as the elastic rod model of DNA, are the focus of the next two sections. For this effort, we define an *index* of each extremal to be a nonnegative integer that corresponds to the maximal dimension of a space on which the second variation can be made negative. We can use the index of each extremal to readily identify the solutions which satisfy the necessary condition (2.12). Those extremals that have index zero will be called stable.

3. The Conjugate Point Method

In this section, we summarize the theory of conjugate points for isoperimetrically constrained problems, as described in Manning *et al.* (1998). Bolza (1973), citing work of Weierstrass and Kneser, shows that condition (2.12) is equivalent to an equilibrium having no conjugate point, where $\sigma < 1$ is called a conjugate point for an isoperimetric problem if the following system has a nontrivial solution:

$$\begin{aligned} &\mathcal{S}\boldsymbol{\zeta} + \sum_{i=1}^{n} c_i \mathbf{T}_i = 0 \quad 0 < s < \sigma, \ \text{ for some constants } c_i, \\ &\boldsymbol{\zeta}(0) = \boldsymbol{\zeta}(\sigma) = \mathbf{0}, \quad \int_0^\sigma \boldsymbol{\zeta}^T \mathbf{T}_i \, \mathrm{d}s = 0, \ \ i = 1, \ldots, n. \end{aligned} \tag{3.1}$$

We embed the conjugate point definition into the family of eigenvalue problems

$$\begin{aligned} &\mathcal{S}\boldsymbol{\zeta} + \sum_{i=1}^{n} c_i \mathbf{T}_i = \rho\boldsymbol{\zeta}, \quad 0 < s < \sigma, \ \text{ for some constants } c_i, \\ &\boldsymbol{\zeta}(0) = \boldsymbol{\zeta}(\sigma) = \mathbf{0}, \quad \int_0^\sigma \boldsymbol{\zeta}^T \mathbf{T}_i \, \mathrm{d}s = 0, \ \ i = 1, \ldots, n. \end{aligned} \tag{3.2}$$

where conjugate points are values of $\sigma < 1$ such that the eigenvalue problem (3.2) has a zero eigenvalue. For unconstrained problems, Morse (1951) showed that the Morse index exactly corresponds to the number of conjugate points. Using different methods, Manning *et al.* (1998) showed that the index associated with the solutions to an isoperimetrically constrained problem exactly corresponds to the number of conjugate points as defined by (3.1). They also propose an efficient numerical algorithm for solving (3.1) in terms of a matrix of initial value problems, thus providing a practical method for determining the index.

In certain cases, the equation (3.1) has special features that allow for a simplification of the conjugate point problem. In particular, for circular solutions to the elastic loop problem, (3.1) is constant coefficient and can be solved analytically, thereby giving an analytical determination of the conjugate points. Alternatively, if

the bifurcation parameter appears linearly in the functional (instead of appearing in the boundary conditions as in (2.4)), then parameter values for which (3.1) has a nontrivial solution at $\sigma = 1$ determine where the index changes. The value of the index for parameter values in between these distinct parameter values can be determined based on the sign of a particular inner product. Such a situation arises, for instance, in the elastic rod model of a twisted DNA filament subject to endloading (see Hoffman *et al.* 2002).

4. The Distinguished Diagram Method

Consider a family of solutions to (2.5). Folds are points in the family of solutions at which the bifurcation parameter passes through a local extreme value. Standard bifurcation theory asserts that (generically) stability exchanges occur at folds. In particular, if one branch of a simple fold is known to represent stable solutions, then the other branch represents unstable solutions. Exploiting the underlying variational structure of elastic rod theory, for example, this classic stability exchange result can be strengthened to predict the *direction* of stability exchange from the shape of certain particular projections of the solution set (Maddocks 1987; Thompson 1979). Previous work assumed that the bifurcation parameter was in the functional and in the case of the isoperimetrically constrained calculus of variations problem was the Lagrange multiplier. For the elastic rod model of DNA minicircles, the bifurcation parameter α appears in the boundary conditions of the constrained problem. In this section, we derive the ordinate of the distinguished bifurcation diagram for calculus of variations problems of the type (2.4). For further details and generalizations of the theory, see Rogers (1997).

We begin by demonstrating that the eigenvalue problem (3.2) has a zero eigenvalue $\rho = 0$ at a fold in the bifurcation parameter. Differentiating the Euler-Lagrange equations (2.5), the integral constraints and the nonlinear boundary conditions (2.4) with respect to pseudo-arclength τ along the branch and subsequently projecting using $\mathbf{\Pi}$ yields the constrained boundary value problem

$$\begin{gathered} \mathcal{S}\dot{\boldsymbol{\eta}} + \sum_{i=1}^{n} \dot{\lambda}_i \mathbf{T}_i = \mathbf{0}, \\ \dot{\boldsymbol{\eta}}(0) = \mathbf{0}, \;\; \dot{\boldsymbol{\eta}}(1) = \hat{\mathbf{f}}(\alpha)\dot{\alpha}, \;\; \int_0^1 \dot{\boldsymbol{\eta}}^T \mathbf{T}_i \, \mathrm{d}s = 0, \;\; i = 1, \ldots, n, \end{gathered} \tag{4.1}$$

where $\hat{\mathbf{f}} = \mathbf{\Pi}\frac{\mathrm{df}}{\mathrm{d}\alpha}$ and $\dot{\boldsymbol{\eta}} = \mathbf{\Pi}\dot{\mathbf{q}}$. The constrained boundary value problems (3.1) and (4.1) are identical (with $c_i = \dot{\lambda}_i, \dot{\boldsymbol{\eta}} = \boldsymbol{\zeta}, \sigma = 1$) provided $\dot{\alpha} = 0$. If we let $\boldsymbol{\zeta}$ denote the eigenvector and ρ denote the eigenvalue of (3.2) along a curve of solutions, then at fold points in the parameter, $\rho = 0$ and $\boldsymbol{\zeta} = \dot{\boldsymbol{\eta}}$ for $\sigma = 1$.

If we further assume that $\rho = 0$ is a simple eigenvalue at the fold, then we can derive an expression for $\dot{\rho}$ by taking the inner product of equation (4.1) with $\boldsymbol{\zeta}$

$$\langle \boldsymbol{\zeta}, \mathcal{S}\dot{\boldsymbol{\eta}} \rangle + \sum_{i=1}^{n} \dot{\lambda}_i \langle \boldsymbol{\zeta}, \mathbf{T}_i \rangle = 0$$

and integrating the first term $\langle \boldsymbol{\zeta}, \mathcal{S}\dot{\boldsymbol{\eta}} \rangle$ by parts:

$$\langle \mathcal{S}\boldsymbol{\zeta}, \dot{\boldsymbol{\eta}} \rangle + \boldsymbol{\zeta}'(1) \cdot \mathbf{P}\hat{\mathbf{f}}\dot{\alpha} + \sum_{i=1}^{n} \dot{\lambda}_i \langle \boldsymbol{\zeta}, \mathbf{T}_i \rangle = 0. \tag{4.2}$$

Rewriting $\mathcal{S}\boldsymbol{\zeta} = \rho\boldsymbol{\zeta} - \sum_{i=1}^{n} c_i \mathbf{T}_i$ from (3.2) allows (4.2) to be expressed as

$$\langle \rho\boldsymbol{\zeta}, \dot{\boldsymbol{\eta}} \rangle - \sum_{i=1}^{n} c_i \langle \mathbf{T}_i, \dot{\boldsymbol{\eta}} \rangle + \boldsymbol{\zeta}'(1) \cdot \hat{\mathbf{P}}\hat{\mathbf{f}}\dot{\alpha} + \sum_{i=1}^{n} \dot{\lambda}_i \langle \boldsymbol{\zeta}, \mathbf{T}_i \rangle = 0.$$

The terms involving $\langle \dot{\boldsymbol{\eta}}, \mathbf{T}_i \rangle$ and $\langle \boldsymbol{\zeta}, \mathbf{T}_i \rangle$ vanish since by definition, each eigenvector along the curve of solutions is orthogonal to $\mathbf{T}_i$ (for $\sigma = 1$) and the eigenvalue ρ has the following representation:

$$\rho \langle \boldsymbol{\zeta}, \dot{\boldsymbol{\eta}} \rangle + \boldsymbol{\zeta}'(1) \cdot \mathbf{P}\hat{\mathbf{f}}\dot{\alpha} = 0.$$

Differentiating this equation with respect to pseudo-arclength τ

$$\dot{\rho}\langle \boldsymbol{\zeta}, \dot{\boldsymbol{\eta}} \rangle + \rho \frac{\mathrm{d}}{\mathrm{d}\tau} \langle \boldsymbol{\zeta}, \dot{\boldsymbol{\eta}} \rangle = -\ddot{\alpha}\boldsymbol{\zeta}'(1) \cdot \mathbf{P}\hat{\mathbf{f}} - \dot{\alpha} \frac{\mathrm{d}}{\mathrm{d}\tau} \left[\boldsymbol{\zeta}'(1) \cdot \hat{\mathbf{P}}\hat{\mathbf{f}} \right]$$

and evaluating at a fold ($\rho = 0,\ \boldsymbol{\zeta} = \dot{\boldsymbol{\eta}},\ \dot{\alpha} = 0$) yields the expression

$$\dot{\rho}\langle \dot{\boldsymbol{\eta}}, \dot{\boldsymbol{\eta}} \rangle = -\ddot{\alpha}\ \dot{\boldsymbol{\eta}}'(1) \cdot \hat{\mathbf{P}}\hat{\mathbf{f}}. \tag{4.3}$$

The definition of pseudo-arclength implies that $\langle \dot{\boldsymbol{\eta}}, \dot{\boldsymbol{\eta}} \rangle = 1$ at a fold. It can be shown that $\dot{\boldsymbol{\eta}}'(1) \cdot \hat{\mathbf{P}}\hat{\mathbf{f}}$ is the perfect derivative with respect to pseudo-arclength of $\mathbf{\Pi} E_{\mathbf{q}'} \cdot \hat{\mathbf{f}}$ evaluated at $s = 1$. Remarkably, this expression simplifies to $\dot{m}_3(1)$ for general models of twisted elastic rods such as (2.4). Therefore, we conclude that

$$\dot{\rho} = -\ddot{\alpha}\dot{m}_3(1). \tag{4.4}$$

Consider a plot of a curve of solutions to (2.5) with a fold. At the fold point we have shown that the eigenvalue of (3.2) is zero. Equation (4.4) determines whether the eigenvalue is increasing or decreasing. The sign of $\ddot{\alpha}$ is determined by whether the fold opens to the right ($\ddot{\alpha} > 0$) or the left ($\ddot{\alpha} < 0$). The term $\dot{m}_3(1)$ assigns a direction to the pseudo-arclength of the curve, that is, the arclength increases as the curve is traversed from the lower branch to the upper branch. As a result, for a fold opening to the right, the eigenvalue is decreasing at the fold, and the upper branch has at least one negative eigenvalue and therefore those solutions cannot correspond to minima. A similar arguement holds for folds opening to the left. See figure 2*a* for examples of stability exchanges at folds opening to both the right and the left.

The ordinate of the distinguished diagram involves m_3 which is not a quantity that can be measured experimentally. The distinguished diagram can be reinterpreted in terms of more biologically reasonable quantities. For instance, instead of plotting m_3 as a function of the parameter α, one could plot the energy E as a function of link Lk, which are more biologically intuitive quantities (Hoffman *et al.* 2003).† Folds in the bifurcation parameter α correspond to cusps in the $E - Lk$

† Applied to cyclized DNA minicircles, the quantity Lk is known to be an integer. However, the definition can be extended to "nicked" DNA where the frame of the elastic rod model does not close (Fuller 1978, Hoffman *et al.* 2003).

diagram. Stability information can be derived by a careful analysis of the stability information in the $m_3 - \alpha$ diagram and the relationship between these variables and $E - Lk$. For the $E - Lk$ diagram, the higher energy branch has the higher index and therefore cannot correspond to a minimum. In the next section, two examples are presented that demonstrate the distinguished diagram method. For the example of a DNA minicircle, the distinguished diagram involving E and Lk is plotted, whereas α and m_3 are plotted for the example of the DNA filament.

5. Examples

In this section we present two examples: a DNA minicircle with a catabolite gene activator protein (CAP) binding site and a DNA filament with an A-tract. In each example, the DNA molecules were built using sequence information about A-tracts and CAP binding sites derived from the literature. Once the sequence structure of the molecule was known, the unstressed shapes of the discretized molecule were computed using a modified version of the classical Trifonov angles (Kahn & Crothers 1998). From this information about the discrete molecule, appropriate averaging and filtering yields the functions $\hat{u}_1(s), \hat{u}_2(s), \hat{u}_3(s)$, which are inputs into the continuous model (Manning *et al.* 1996). Once the input functions $\hat{u}_1(s), \hat{u}_2(s), \hat{u}_3(s)$ were known, a family of equilibria of the elastic rod model of the molecule was computed using the boundary-value problem solver AUTO (Doedel (1991a, b)). The index of each equilibrium along the branch of solutions was determined using the conjugate point method and the distinguished diagram was plotted. The results are shown in figures 1 and 2.

(*a*) *DNA Minicircle with CAP binding site*

In this example, we construct a 162bp DNA molecule with a Escherichia coli CAP binding site beginning at the 81^{st} basepair. The CAP binding sequence consists of 22 bp with two-fold symmetry: 5'-AAA TGT GAT CTAG ATC ACA TTT-3' (Gunasekera *et al.* (1992)). The remainder of the molecule consists of seven copies of the sequence: 5'-CCG GAT CCGT ACAG GAA TTC-3', which was used as an adaptor sequence by Kahn & Crothers (1992). This sequence leads to input functions $\hat{u}_1, \hat{u}_2$ that describe an essentially straight elastic rod, whereas the CAP site sequence creates a slight bend in the unstressed molecule. In this example, the protein is not actually bound to the molecule–such a binding would induce a dramatic bend in the unstressed molecule.

Once the functions $\hat{u}_i$ were determined, the equilibrium solutions of the elastic rod model were computed with $\gamma = K_3/K_1 = 1.6$ for varying amounts of imposed twist. The index of each solution was then computed using the conjugate point method. In this case, the resulting bifurcation diagram displayed in figures 1 a, b is presented in terms the biological quantities of energy and linking number. These diagrams demonstrates that stability changes occur at cusps in the $E - Lk$ diagram and that the branch with the higher energy has the higher index. Figures 1b, c displays two different projections of a stable nonplanar circular loop. This particular configuration could represent a DNA minicircle since the frame, as well as the centerline, of the elastic rod model is closed.

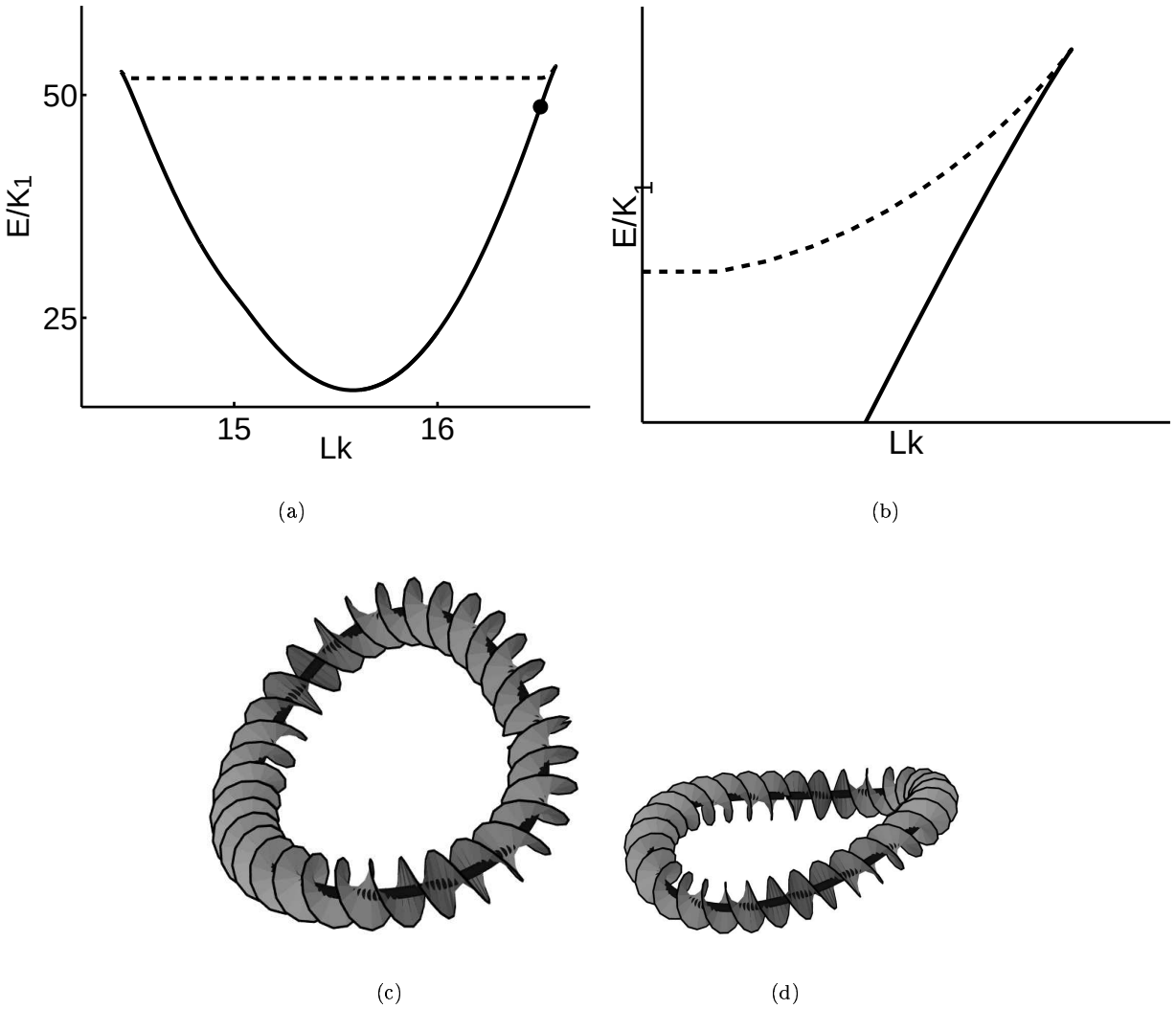

Figure 1. Figure (a) displays the $E - Lk$ bifurcation diagram of a DNA minicircle with an Escherichia coli CAP binding site. Figure (b) depicts the cusp in the upper right of figure 1 (a). The line style indicates the index of the solutions: the solid line corresponds to index zero solutions and the dashed line corresponds to index one solutions. The index was computed using the conjugate point method and demonstrates that the stability changes at cusps in the $E - Lk$ bifurcation diagram. Figure 1 (c) and (d) illustrate two projections of the stable solution that corresponds to the point marked with a solid circle in figure 1 (a).

(b) *DNA Filament with an A-tract*

A DNA filament is constructed with an A-tract bend at the centre of the filament. The molecule consists of 179bp with six A-tracts. The remainder of the molecule was constructed with six copies of the sequence 5'-CCG GAT CCGT

ACAG GAA TTC-3', which was used in the previous example. Thus, the molecule is described by an essentially straight elastic rod with a bend at the centre induced by the A-tract. The equilibrium solutions were computed for varying twist, with constant tension at the $s = 1$ end of the elastic rod and $\gamma = 1.6$. The results are shown in figure $2a$, where the distinguished bifurcation diagram $m_3 - \alpha$ has been plotted, showing the stability exchange for folds in both directions. Figure $2b, c$ displays two projections of a stable nonplanar configuration.

6. Discussion

We have presented two methods for determining the stability of equilibria of elastic rod models of DNA. The methods can be used on a wide class of problems that encompass many biological properties of the molecule. In this article, two examples were presented that illustrate the techniques on inherently curved molecules, although many other features may be incorporated. A model of DNA that would better reflect the biology would incorporate an electrostatic repulsion on the elastic rod (Westcott *et al.* 1997, Yang *et al.* 1995), thus producing an infinite energy barrier as non-adjacent points on the rod come in close proximity. Bulman & Manning (unpublished work) have developed and implemented a conjugate point method to determine the stability of an elastic rod as it approaches a wall with a repulsive potential. We believe that similar techniques can be used to determine stability for an elastic rod model of DNA with an electrostatic self-repulsive force.

The conjugate point method determines the index of a particular solution whereas the distinguished diagram determines instability of a family of solutions by identifying branches of solutions whose index are at least one. In order to determine stability using the distinguished diagram method, the index of at least one solution on the branch must be determined by other methods, such as the conjugate point method. Thus, for computationally intensive problems, the methods are complementary in that the conjugate point test can be used to determine the stability of one solution, then the distinguished diagram can be used to draw stability conclusions for the remaining solutions along the branch.

Although the nature of the two stability methods is quite different, the same principle underlies both methods. Both methods are tracking eigenvalues of a projected eigenvalue problem

$$\begin{aligned} \mathcal{Q}\mathcal{S}\mathcal{Q}\boldsymbol{\zeta} &= \rho\boldsymbol{\zeta}, \quad 0 < s < \sigma, \\ \boldsymbol{\zeta}(0) = \boldsymbol{\zeta}(\sigma) &= \mathbf{0}, \quad \int_0^\sigma \boldsymbol{\zeta}^T \mathbf{T}_i \, \mathrm{d}s = 0, \quad i = 1, \ldots, n, \end{aligned} \tag{6.1}$$

where $\mathcal{Q}$ is a projection operator onto the L^2-orthogonal complement of $\mathrm{span}(\mathbf{T}_1, \ldots, \mathbf{T}_n)$ (Manning *et al.* 1998). The conjugate point method tracks the eigenvalues of (6.1), which is equivalent to (3.2), for a range of σ values, whereas, the distinguished diagram method predicts sign changes in the eigenvalue for $\sigma = 1$ along families of solutions. For the two examples presented here, the index was computed using the conjugate point method for a family of solutions and the number of negative eigenvalues changed at folds in the bifurcation parameter, as predicted by the distinguished diagram theory. Moreover, the additional conjugate point associated with negative eigenvalue that is gained as a fold is traversed, arises from the zero eigenvalue at a fold for $\sigma = 1$. This implies that changes in the index occur at parameter

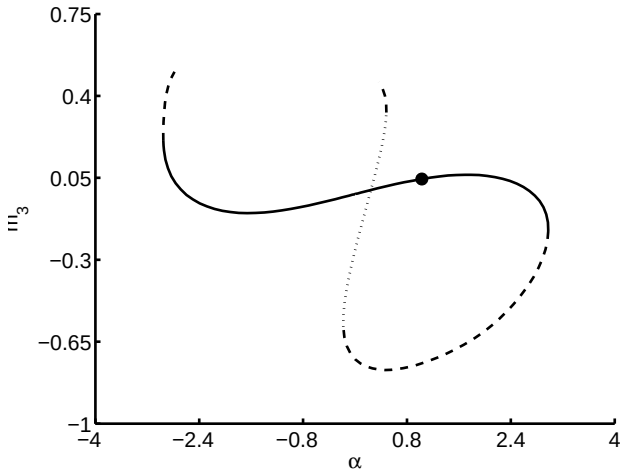

(a)

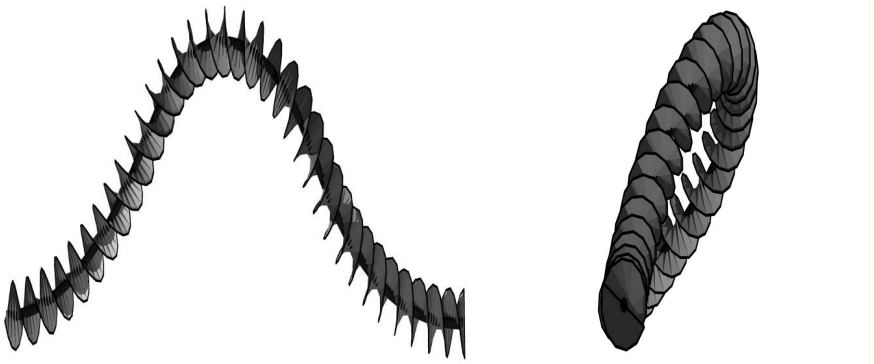

(b) (c)

Figure 2. Figure 2 (*a*) displays the $m_3 - \alpha$ bifurcation diagram of a DNA filament with an A-tract bend at the centre. The line style indicates the index of the solutions as stated in the caption of figure 1, with the dotted line corresponding to configurations with index two. The apparent crossing of the solid line with the dotted line is an artefact of this projection of the bifurcation diagram and does not represent an actual crossing. The stability changes at folds exactly as predicted by the distinguished diagram theory. The figures 2 (*b*) and (*c*) illustrates two projections of a stable, hence biologically accessible, solution indicated in (a) by the solid circle.

values that have a conjugate point at $\sigma = 1$. The index can be determined by knowing the index at one parameter value, as in the distinguished diagram theory. This was proved for a specific example of the elastic strut (Hoffman *et al.* 2002), but is not true for elastic rods with more general boundary conditions (Bulman & Manning, unpublished work).

It is my pleasure to extend my deepest appreciation to Rob Manning for his help with the examples in this manuscript as well as for many helpful discussions. I would also like to thank John Maddocks for introducing me to the fascinating field of mechanical models of DNA and for sharing his knowledge, intuition and insights on constrained variational principles.

References

Antman. S. S. 1995 *Nonlinear problems of elasticity.* New York: Springer-Verlag.

Benham, C.J. 1989 Onset of writhing in circular elastic polymers. *Phys. Rev. A* **39**(5), 2582–2586.

Bolza, O. 1973 *Lectures on the calculus of variations.* New York: Chelsea Publishing Company.

Bouchiat, C. & Mezard, M. 2000 Elastic rod model of a supercoiled DNA molecule. *Eur. Phys. J. E* **2**, 367–376.

Coleman, B., Swigon, D., & Tobias, I. 2000 Elastic stability of DNA configurations. II. Supercoiled plasmids with self-contact. *Phys. Rev. E* **61**, 759–770.

Dichmann, D.J. 1994 Hamiltonian dynamics of a spatial elastica and the stability of solitary waves. Ph.D. thesis, University of Maryland, College Park.

Dichmann, D.J., Li, Y.W., & Maddocks, J.H. 1996 Hamiltonian formulations and symmetries in rod mechanics. In *Mathematical approaches to biomolecular structure and dynamics* (ed. J.P. Mesirov, K. Schulten & D.W. Sumners). IMA volumes in mathematics and its applications **82**, 71–113.

Doedel, E.J., Keller, H.B. & Kernvez, J.P. 1991*a* Numerical analysis and control of bifurcation problems: (I) Bifurcation in finite dimensions. *Int. J. Bifurcation & Chaos* **1**, 493–520.

Doedel, E.J., Keller, H.B. & Kernvez, J.P. 1991*b* Numerical analysis and control of bifurcation problems: (II) Bifurcation in infinite dimensions. *Int. J. Bifurcation & Chaos* **1**, 745–772.

Fuller, F. B. 1978 Decomposition of the linking number of a closed ribbon:A problem from molecular biology *Proc. Natl. Acad. Sci* **75** (8), 3557–3561.

Goriely, A. & Tabor, M. 1997*a* Nonlinear dynamics of filaments I: Dynamical instabilities. *Physica D* **105**, 45–61.

Goriely, A. & Tabor, M. 1997*b* Nonlinear dynamics of filaments II: Nonlinear analysis. *Physica D* **105**, 20–44.

Goriely, A. & Tabor, M. 1997*c* Nonlinear dynamics of filaments III: Instabilities of helical rods. *Proc. Roy. Soc* **453**, 2583–2601.

Guitter, E. & Leibler, S. 1992 On supercoiling instability in closed DNA. *Europhysics Letters* **17**(7), 643–648.

Gunasekera, A. Ebright Y. W., Ebright, R.H. 1992. DNA sequence determinants for binding of the escherichia coli catabolite gene activator protein. *The Journal of Biological Chemistry*, 267:14713-14720.

Hagerman, P. 1988 Flexibility of DNA. *Ann. Rev. Biophys. Biophys. Chem.* **17**, 265–286.

Hestenes, M.R. 1966 *Calculus of variations and optimal control theory.* Robert E. Krieger Publishing Co.

Hoffman, K.A., Manning, R.S. & Maddocks, J.H. 2003 Biological interpretations of bifurcation diagrams. *Biopolymers*, vol 70, no 2, p. 145-157.

Hoffman, K.A., Manning, R.S. & Paffenroth, R.C. 2002 Calculation of the stability index in parameter-dependent calculus of variations problems: Buckling of a twisted elastic strut. *SIAM J. Applied Dyn. Sys.* **1**, 115–145.

Jülicher, F. 1994 Supercoiling transitions of closed DNA *Phys. Rev. E* **49** (3), 2429–2435.

Kahn, J.D. & Crothers, D.M. 1992 Protein-induced bending and DNA cyclization. *Proc. Natl. Acad. Sci.* **89**, 6343–6347.

Kahn, J.D. & Crothers, D.M. 1998 Measurement of the DNA bend angle induced by the catabolite activator protein using Monte Carlo simulation of cyclization kinetics. *J. Mol. Biol.* **276**, 287–309.

Kehrbaum, S., Maddocks, J.H. 2000 Effective properties of elastic rods with high intrinsic twist. In *Proceedings of the 16th IMACS World Congress 2000* (ed. M. Deville & R. Owens).

LeBret, M. 1979 Catastrophic variation of twist and writhing of circular DNAs with constraint? *Biopolymers* **18**, 1709-1725.

LeBret, M. 1984 Twist and writhing in short circular DNA according to first-order elasticity. *Biopolymers* **23**, 1835–1867.

Maddocks, J.H. 1987 Stability and folds. *Arch. for Rat. Mech. & Anal.* **85**, 180-198.

Manning, R.S., Maddocks, J.H. & Kahn J.D. 1996 A continuum rod model of sequence-dependent DNA structure. *J. Chem. Phys.* **105**, 5626–5646.

Manning, R.S., Rogers, K.A., & Maddocks, J.H. 1998 Isoperimetric conjugate points with application to the stability of DNA minicircles. *Proc. R. Soc. London A* **454**, 3047–3074. (K. A. Hoffman née K. A. Rogers).

Manning, R.S., & Hoffman, K.A. 2001 Stability of n-covered circles for elastic rods with constant planar intrinsic curvature. *J. Elasticity* **62**, 1–23.

Michell, J.H. 1889 On the stability of a bent and twisted wire. *Messenger of Mathematics* **19**, 181–184.

Moroz, J.D. & Nelson, P. 1998 Entropic elasticity of twist-storing polymers. *Macromolecules* **31**, 6333–6347.

Morse, M. 1951 *Introduction to analysis in the large.* Institute for Advanced Study.

Neukirch, S, van der Heijden, G., & Thompson, J.M.T. 2002 Writhing instabilities of twisted rods: From infinite to finite length. *Journal of the Mechanics and Physics of Solids* **50**, 1175–1191.

Olson, W.K. 1996 Simulating DNA at low resolution. *Current Opinion in Structural Biology* **6**,242–256.

Rey, S., Maddocks, J.H. 2000 Buckling of an elastic rod with high intrinsic twist. In *Proceedings of the 16th IMACS World Congress 2000* (ed. M. Deville & R. Owens).

Rogers, K.A. 1997 Stability exchange in parameter-dependent constrained variational principles with applications to elastic rod models of DNA minicircles. Ph.D. thesis, University of Maryland, College Park. (K.A. Hoffman née K.A. Rogers).

Schlick, T. 1995 Modeling superhelical DNA: Recent analytical and dynamical approaches. *Current Opinion in Structural Biology* **5**, 245–262.

Smith, S., Cui, Y. & Bustamante, C. 1996 Overstretching B-DNA: The elastic response of individual double-stranded and single-stranded DNA molecules. *Science* **271**,795–799.

Thompson, J.M.T. 1979 Stability predictions through a succession of folds. *Phil. Trans. Roy. Soc. London, Series A, Math. and Phys. Sci.*. **292**, 1–23.

Tobias,I., Swigon, D., & Coleman, B. 2000 Elastic stability of DNA configurations I: General theory. *Phys. Rev. E* **61**, 747–758.

van der Heijden, G., Neukirch, S, Goss,V. G. A. & Thompson, J.M.T. 2003 Instability and self-contact phenomena in the writhing of clamped rods. *International Journal of Mechanical Science* **45**, 161–196.

Watson, J.D. & Crick, F.H.C. 1953 Molecular structure of nucleic acids. A structure for deoxyribose nucleic acid. *Nature* **171**, 737–738.

Westcott, Timothy P., Tobias, Irwin, & Olson, Wilma K. 1997 Modeling self-contact forces in the elastic theory of DNA supercoiling. *J. Chem. Phys.* **107**, 3967–3980.

Yang, Y., Tobias, I., & Olson, W.K. 1993 Finite element analysis of DNA supercoiling. *J. Chem. Phys.* **98**, 1673-1686.

Yang, Y., Westcott, T. P., Pedersen, S. C., Tobias, I., and Olson, W. K. 1995 The effect of sequence-directed bending on DNA supercoiling. *Trends in the Biochemical Sciences* **20**, 313–319.

Zajac, E.E. 1962 Stability of two planar loop elasticas. *J. Applied Mechanics (Trans ASME, Series E).* **29**, 136–142.